ACSNANO

www.acsnano.org

ARTICLE

Light-Triggered Mechanical Disruption of Extracellular Barriers by Swarms of Enzyme-Powered Nanomotors for Enhanced Delivery

Juan C. Fraire,* Maria Guix, Ana C. Hortelao, Noelia Ruiz-González, Anna C. Bakenecker, Pouria Ramezani, Charlotte Hinnekens, Félix Sauvage, Stefaan C. De Smedt, Kevin Braeckmans,* and Samuel Sánchez*

Cite This: *ACS Nano* 2023, 17, 7180–7193

Read Online

ACCESS | Metrics & More | Article Recommendations | Supporting Information

ABSTRACT: Targeted drug delivery depends on the ability of nanocarriers to reach the target site, which requires the penetration of different biological barriers. Penetration is usually low and slow because of passive diffusion and steric hindrance. Nanomotors (NMs) have been suggested as the next generation of nanocarriers in drug delivery due to their autonomous motion and associated mixing hydrodynamics, especially when acting collectively as a swarm. Here, we explore the concept of enzyme-powered NMs designed as such that they can exert disruptive mechanical forces upon laser irradiation. The urease-powered motion and swarm behavior improve translational movement compared to passive diffusion of state-of-the-art nanocarriers, while optically triggered vapor nanobubbles can destroy biological barriers and reduce steric hindrance. We show that these motors, named Swarm 1, collectively displace through a microchannel blocked with type 1 collagen protein fibers (barrier model), accumulate onto the fibers, and disrupt them completely upon laser irradiation. We evaluate the disruption of the microenvironment induced by these NMs (Swarm 1) by quantifying the efficiency by which a second type of fluorescent NMs (Swarm 2) can move through the cleared microchannel and be taken up by HeLa cells at the other side of the channel. Experiments showed that the delivery efficiency of Swarm 2 NMs in a clean path was increased 12-fold in the presence of urea as fuel compared to when no fuel was added. When the path was blocked with the collagen fibers, delivery efficiency dropped considerably and only depicted a 10-fold enhancement after pretreatment of the collagen-filled channel with Swarm 1 NMs and laser irradiation. The synergistic effect of active motion (chemically propelled) and mechanical disruption (light-triggered nanobubbles) of a biological barrier represents a clear advantage for the improvement of therapies which currently fail due to inadequate passage of drug delivery carriers through biological barriers.

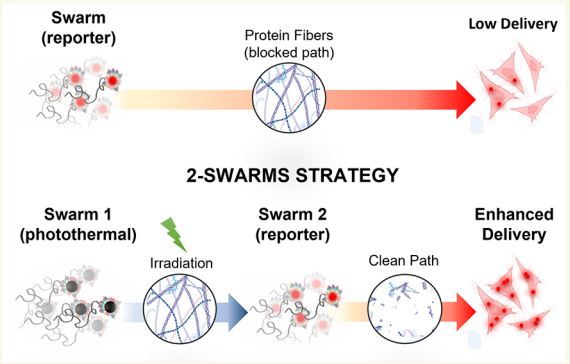

KEYWORDS: *nanomotors, swarming, enzyme catalysis, drug delivery, vapor nanobubbles, nanoparticles*

Nanotechnology-enabled drug delivery systems had undergone substantial evolution in the last few decades driven by the promise of being able to selectively deliver therapeutic molecules to target tissues and cells with increased efficacy, thus reducing side effects. However, despite decades of research and optimization of nanocarrier design, it still remains a challenge to efficiently cross biological barriers between the administration site and the target cell or tissue.[1] Examples of such biological barriers are the mucus layers, extracellular matrices, basement membranes and others.[2] Intracellular barriers such as the plasma membrane, endosomal membranes, and the nuclear envelope also need to be taken into account.[3] In general, nanocarriers must overcome two major limitations for crossing the different barriers: (1) passive diffusion and (2) steric hindrance. Scientists from multidisciplinary teams in the nanotechnology field have combined their efforts to tackle the hurdles associated with the first limitation by exploiting the use of nanoparticles (NPs) with autonomous motion,

Received: September 20, 2022
Accepted: April 4, 2023
Published: April 14, 2023

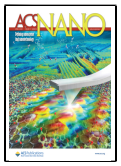

https://doi.org/10.1021/acsnano.2c09380
ACS Nano 2023, 17, 7180–7193

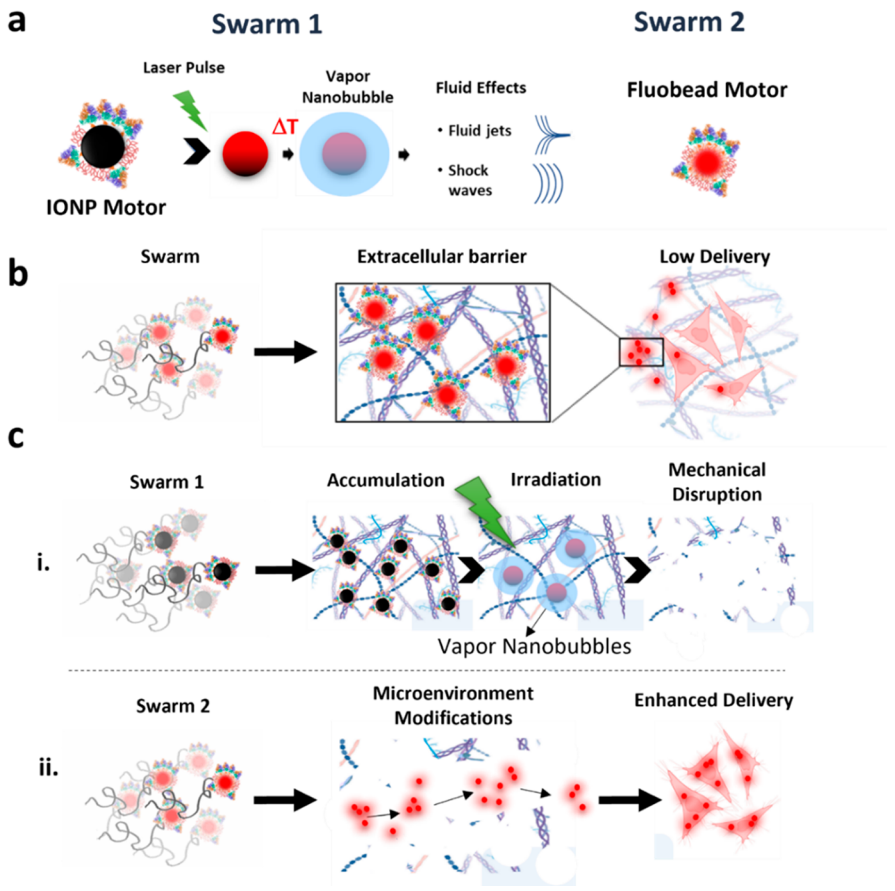

Figure 1. Swarms of nanomotors for enhanced delivery. (a) 500 nm iron oxide nanoparticles (IONPs) and 200 nm red fluorescent polystyrene beads (Fluobead) were used as chassis for the synthesis of Swarm 1 and Swarm 2 of urease-powered nanomotors, respectively. IONP motors form VNBs upon pulsed laser irradiation, inducing fluid jets and shockwaves. (b) Shielding effect of an extracelullar barrier on the delivery of swarms of Fluobead motors. (c) Schematic representation of enzyme-powered nanomotor swarms strategy for enhanced delivery: (i) Swarm 1 will penetrate the extracellular barriers encountered in the path to reach target cells; after accumulation, they will be irradiated, resulting in the barrier disruption; (ii) microenvironment modifications generated by Swarm 1 will allow Swarm 2 to access the target cells (enhanced delivery).

nanomotors (NMs), as the next generation of robotic platforms in nanomedicine to rapidly delivering drug carriers to target locations.[4,5]

Synthetic NMs based on a plethora of different propulsion mechanisms have been explored, including chemically powered motors[6,7] and motors powered by external physical stimuli (e.g., magnetic, acoustic, light).[5] While such systems have exciting prospects, like enhanced drug delivery efficiency when compared to passive particles,[8−11] most of these studies have been carried out in simple 2D cell cultures. However, in more realistic scenarios, biological barriers can be present between the site of administration and the target cells. Therefore, the sole active motion of drug-loaded NM carriers might not be enough to confer the capability to trespass the barriers. Different strategies have been explored to improve the drug delivery performance of NMs by tackling, in parallel the steric hindrance limitation, from NM surface modifications[12−14] to the incorporation of advanced capabilities upon external stimuli,[15,16] or even both.[17] Clear examples are surface-modified NMs able to swim through[18] or even degrade[19,20] gel-like viscous fluids and matrices. While these coatings could be used to overcome the steric hindrance of certain biological barriers, the integration of advanced photothermal capabilities to perform a controlled degradation of barriers, are continuously gaining interest. NM carriers with photothermal properties have been proved to be able to penetrate cell membranes,[21−23] cell clusters,[23−25] and even complex matrices like thrombi,[26−28] with improved delivery efficiencies by the thermal degradation induced upon continuous laser irradiation.

Degradation of biological barriers by photothermal means is a topic that is being actively explored in the drug delivery field. Of particular interest is the combination of photothermal NPs and pulsed lasers (typically nanosecond laser pulses), in which a high amount of energy is absorbed upon illumination, inducing a quick heat up of the NPs to several hundred degrees. Consequently, the water of the surrounding environment evaporates to form vapor nanobubbles (VNBs) emerging around the surface of the NPs that will first expand and then collapse, thereby generating fluid jets and high-pressure shockwaves that result in a drastic mechanical disruption of the barriers instead of a soft thermal degradation. Passive photothermal particles for mechanical disruption of biological barriers have been used to induce disruption of biofilms in vitro,[29,30] protein fibers and matrices ex vivo,[31] and even in vivo for tissues easily accessible for laser irradiation.[32]

In this study, we designed enzyme-powered NMs capable of forming laser-induced VNB. Among the different propulsion mechanisms, we chose enzyme-powered motion, since enzymes can use physiologically relevant fuels through catalytic reactions to power motion in in vivo conditions.[4,7,33] In

https://doi.org/10.1021/acsnano.2c09380
ACS Nano 2023, 17, 7180−7193

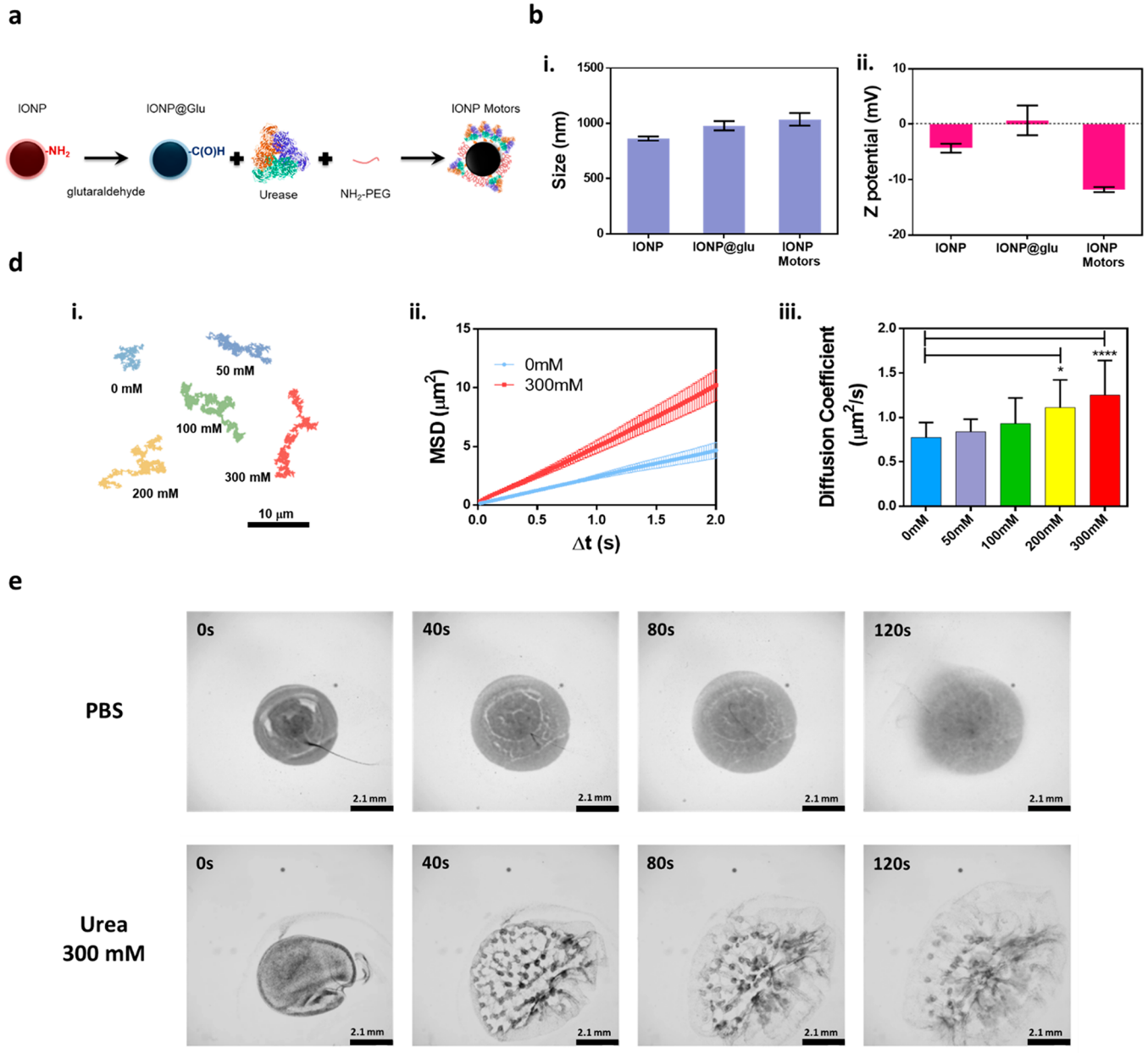

Figure 2. Design, synthesis, motion analysis and in vitro swarming of urease-powered IONP motors. (a) 500 nm IONPs were first functionalized with glutaraldehyde to form IONP@Glu, after which they were co-incubated in the presence of urease and NH_2-PEG-SH to finally form IONP motors. (b) IONP motors physicochemical characterization by (i) dynamic light scattering and (ii) zeta-potential analysis. (c) IONP motors motion analysis: (i) representative tracking trajectories of the nanomotors during 15 s at different urea concentrations; (ii) nanomotors MSD in PBS without and with urea (300 mM) in PBS (N = 15, error bars represent s.e.m.); (iii) diffusion coefficient of nanomotors obtained by optical tracking at different urea concentrations (N = 15; error bars represent standard error of the mean). Superscripts denote statistically significant differences compared to diffusion at 0 mM of urea, with (*) $p < 0.05$ and (****) $p < 0.0001$ (ANOVA test). (d) In vitro swarming analysis of Swarm 1: (d) snapshots of a IONP motors population in PBS (top row) and in 300 mM urea in PBS (bottom row). Scale bar, 2.1 mm.

particular, we made use of urease as it is arguably one of the most promising enzymes for the design of NMs due to its high catalytic turnover rate which confers superior self-propelling capabilities to NMs compared to other enzymes (e.g., acetylcholinesterase, glucose oxidase).[34,35] Moreover, it was demonstrated that urease-powered NMs exhibit collective behavior in the presence of urea as fuel, depicting enhanced fluid mixing and collective displacement forming patterns of high particle densities (we will further refer as swarm formation or swarming to this behavior) in vitro, and enhanced penetration, retention,[36] and even convection and mixing[37] in the bladder in vivo. The main goal of this study is to explore the use of swarms able to induce microenvironment modifications of biological barriers (Swarm 1) shielding target cells, facilitating the delivery of a second swarm (Swarm 2). To that end, we designed two different swarms of NMs (Figure 1a): (1) urease functionalized 500 nm iron oxide nanoparticles (IONPs) for the mechanical disruption of barriers by laser-induced VNB formation[38,39] (Swarm 1: IONP motors) and (2) urease functionalized fluorescent polystyrene beads

https://doi.org/10.1021/acsnano.2c09380
ACS Nano 2023, 17, 7180−7193

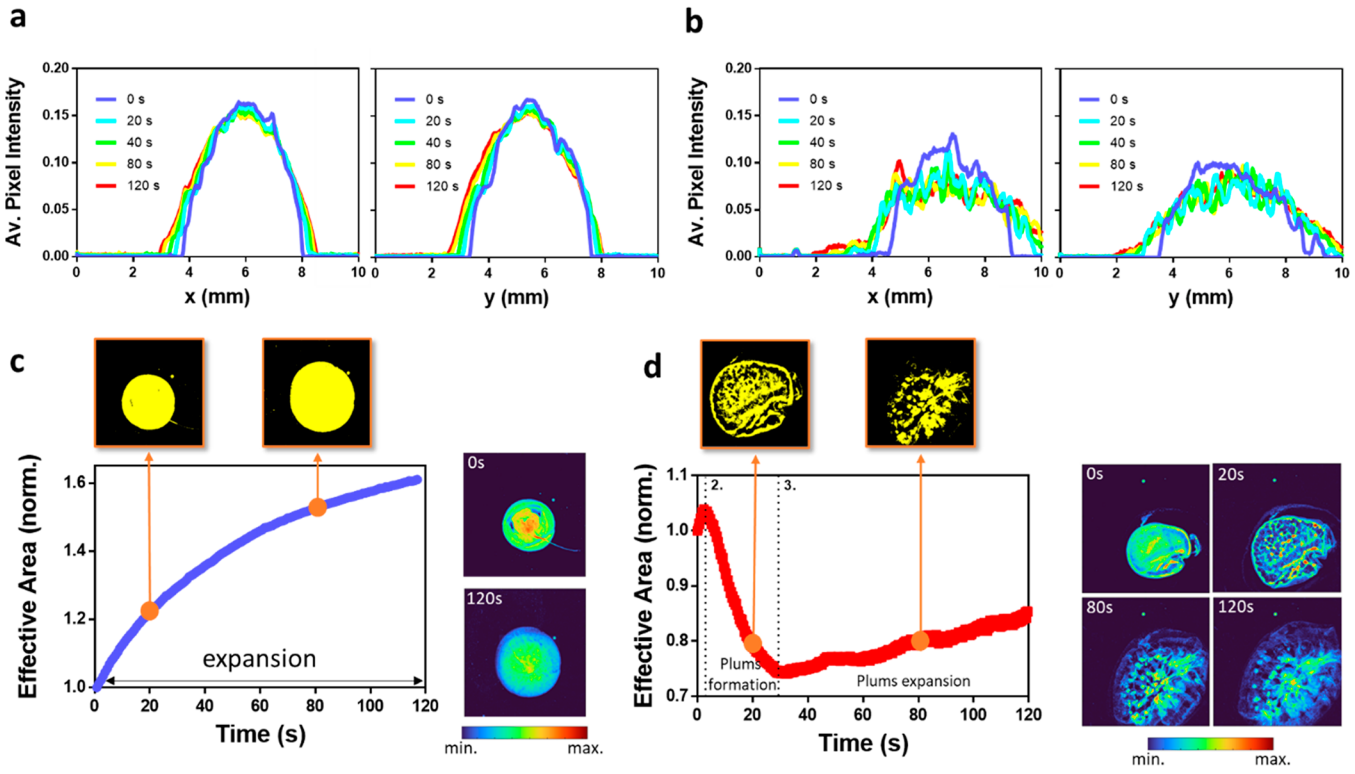

Figure 3. Analysis of the in vitro swarming behavior of urease-powered IONP nanomotors. Projections of the average pixel intensity along the *x*-axis and the *y*-axis for IONP motors (a) in PBS and (b) in 300 mM urea in PBS for selected time points (0, 20, 40, 80, and 120 s). Effective area normalized to the initial area at 0 s occupied by the swarm cloud as a function of time for motors (c) in PBS and (d) in 300 mM urea in PBS. The different regimes of collective behavior observed are highlighted in the graph. The insets depicted with orange arrows correspond to the effective area at the indicated time point (20 and 80 s). Snapshots taken from the background corrected and color coded videos illustrating the pixel intensities of the swarm cloud at 0 and 120 s for nanomotors in PBS and at 0, 20, 80, and 120 s for nanomotors in 300 mM urea in PBS.

(Swarm 2: Fluobead motors) that will act as a reporter system emulating a drug-loaded carrier. We selected type I collagen fibers as a biological barrier model, and we proceeded to determine the laser pulse fluence needed for VNB generation from the IONP core and investigate their disruption. Analysis of the disruption was performed at the single fiber level and by bulk measurements of the rheological properties of a dispersion of fibers. In a next step, we evaluate the collective displacement of the different swarms inside phantom microfluidic channels. The delivery efficiency of Swarm 2 was evaluated in channels filled with collagen fibers using HeLa as cell model (Figure 1b). In the final part of the study, we demonstrate that the swarms with specific functionalities (one for barrier disruption and one for transport of drugs) could induce an overall enhancement of the delivery efficiency by overcoming both passive diffusion and steric hindrance limitations. In that sense, Swarm 1 will accumulate in the biological barrier model, which after laser treatment will lead to the disruption and breakage of the protein fibers (Figure 1ci). Microenvironment modifications generated by Swarm 1 of IONP motors will allow Swarm 2 to access the target cells (Figure 1cii). Compared to nonirradiated samples, full treatment (sequential administration of Swarms 1 and 2, and laser irradiation) depicted a 10-fold increase in the overall delivery efficiency.

RESULTS AND DISCUSSION

Design, Characterization, Motion Analysis, and In Vitro Swarming of Urease-Powered IONP Motors. The design of Swarm 1 consists of a photothermal particle as chassis, coated with urease (Figure 2a). We used commercially available 500 nm magnetic beads, consisting of a polymeric core surrounded with an outer amine functionalized iron oxide layer. We will further refer to these particles as iron oxide nanoparticles (IONP), as the iron oxide shell is the photothermal component required for VNB generation. Amine groups were subsequently activated with glutaraldehyde (Glu). In a next step, IONP@Glu were incubated overnight with urease to allow the covalent binding of the enzyme in the presence of polyethylene glycol (NH_2−PEG-SH). The last one acts as stabilizer during the synthesis of the NMs. The asymmetric distribution of enzymes around the NM surface, that occurs stochastically during the enzyme binding process, allows to observe self-diffusiophoresis in the presence of urea as fuel.[40,41] Figure 2bi shows the DLS characterization of the IONP, including the intermediate IONP@Glu and the final synthesized IONP motor. A slight increase in hydrodynamic size was observed upon NM formation from 862 ± 19 nm to 1036 ± 56 nm. Zeta potential measurements shown in Figure 2bii depicted a slight change of the absolute negative value of the IONP particles after glutaraldehyde functionalization, presumably because of the surface reorganization of charged groups at the IONP surface after glutaraldehyde incorporation (IONP@Glu). After urease functionalization, which is

https://doi.org/10.1021/acsnano.2c09380
ACS Nano 2023, 17, 7180−7193

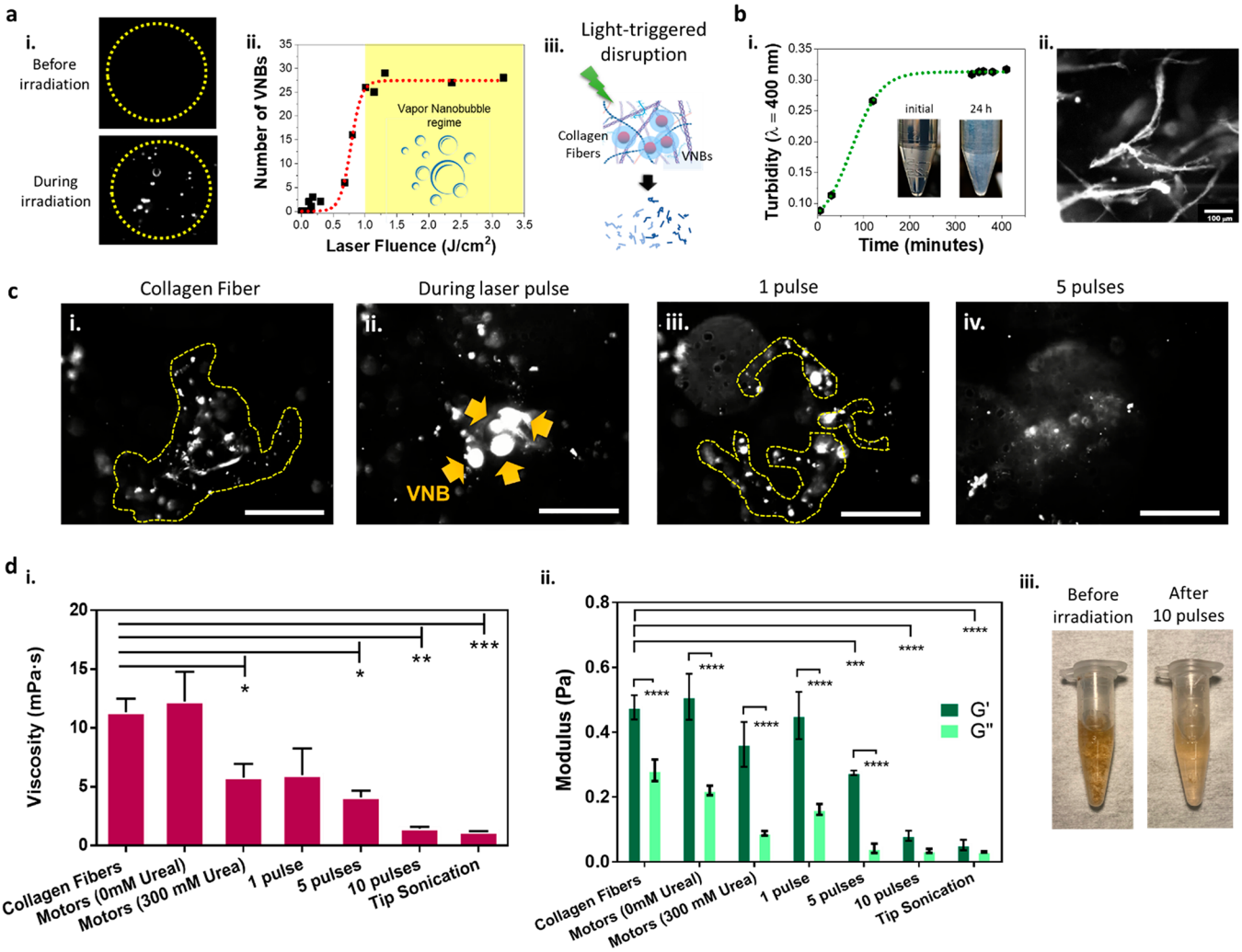

Figure 4. IONP motor-mediated collagen fibers disruption as a biological barrier model. (a) Laser-induced vapor nanobubble formation. (i) Dark-field images before and during a single laser pulse irradiation at the VNB threshold in the presence of IONP motors. (ii) Determination of the VNB fluence threshold for 500 nm IONP motors irradiated with a single 7 ns laser pulse at λ = 561 nm. The VNB regime is indicated in yellow in the graph (0.97 J/cm^2). (iii) Schematic representation of the vapor nanobubble-mediated mechanical collagen fibers disruption in the proximity of the IONP motors. (b) Synthesis and characterization of type I collagen fibers. (i) Turbidity change of a collagen solution, indicating the formation of collagen fibers. Insets correspond to a collagen solution at startpoint of the synthesis and a collagen fibers dispersion after 24 h. (ii) Representative dark-field microscopy image of a collagen fiber in water. (c) Single collagen fiber disruption. Representative dark-field images of collagen fibers previously incubated with IONP motors during 1 h in the presence of urea (300 mM) before (i), during (ii), and after (iii) irradiation with a single laser pulse at the VNB threshold. The perimeter of the fiber or the resulting fragments after disruption and VNBs are highlighted in yellow during irradiation. Scale bars represent 10 μm. (d) Bulk measurements of collagen fibers disruption. Rheometry measurements of (i) the viscosity at a shear rate of 100 (1/s) and (ii) the storage G' and loss G'' modulus at a shear rate of 0.1 (1/s) for 0.01 mg/mL when incubated with IONP motors for 1 h in the presence of urea. Effect of the irradiation when applying 1, 5, or 10 pulses at VNB threshold. Controls include collagen fibers alone, fibers co-incubated with IONP motors without fuel and fibers after tip sonication (20%, 20 s). All results are represented as mean ± SD for n = 3 independent samples. Statistical significance (one-way and two-way ANOVA for (i) and (ii), respectively) is indicated when appropriate (*p < 0.05, **p < 0.01, ***p < 0.001, ****p < 0.0001). (iii) Dispersion of collagen fibers (0.2 mg/mL) after 1 h incubation with IONP motors in the presence of urea before and after 10 pulses irradiation at VNB threshold.

negatively charged at physiological pH, a clear reduction on the zeta-potential was observed to −11.8 ± 0.5 mV for the final NMs. Urease functionalization and its activity after surface binding was further confirmed through a total protein quantification assay and an enzymatic activity test (Supporting Information Figure S1), revealing that at least 95% of the attached enzyme preserves its activity.

Once the activity of urease IONP motors was determined, we performed the corresponding motion analysis using optical microscopy. The NM's motion trajectories were tracked in the absence and presence of different urea concentrations in 1× PBS up to 300 mM (see Figure 2ci), being the maximum urea concentration found in vivo in the bladder.[42] An in-house developed python code was used to analyze the trajectories and compute the mean squared displacement (MSD) as a function of time for each condition. As expected for nanoparticles, for which the rotational diffusion time is very small,[43] the MSD always increased linearly with time, corresponding to enhanced diffusion regime (see representative graphs for 300 mM urea in PBS and the control in absence

https://doi.org/10.1021/acsnano.2c09380
ACS Nano 2023, 17, 7180−7193

of fuel in Figure 2cii). The diffusion coefficients were obtained from linearly fitting the MSD as previously reported (Figure 2ciii).[8,9,44] The IONP motor diffusion coefficient in the absence of urea (Brownian motion) was found to be 0.8 ± 0.1 $\mu m^2/s$. As depicted in the graph, NMs showed a significant increase in the diffusion coefficient dependent on urea concentration, reaching a maximum of 1.3 ± 0.3 $\mu m^2/s$ at 300 mM of urea (increase of 62%). Next, we examined the collective motion dynamics and swarming behavior of the IONP motors in vitro by optical microscopy. For these experiments, 2 μL of NM dispersion (0.01 mg/mL in PBS) was placed at the center of a 3 mL Petri dish, containing either PBS (control) or a 300 mM urea solution in PBS. The corresponding videos were recorded over 2 min (Figure 2di and Movie S1). In the absence of urea, the NMs showed relatively slow diffusion and some sedimentation. In presence of urea, however, vigorous collective motion, referred to as swarming behavior, could clearly be observed. NMs were seen to distribute in an anisotropic manner, forming unstable fronts or "plums", as we will further refer to them, throughout the dish that over time collided and got deposited at the bottom of the dish.

To gain further insight into the swarm dynamics, we first analyzed the projections of the average pixel intensity along the *x*-axis and the *y*-axis of video frames within preestablished time points (0, 20, 40, 80, and 120 s, respectively), as shown in Figure 3a,b. The evolution of the projections of the average pixel intensity along the axes is shown in Movie S2 in the Supporting Information, and correspond to the background corrected videos depicted in Figure 2d and in Movie S1. As shown in Figure 3a, after addition of the droplet of IONP motors in PBS, the nanomotors stay at the seeding point following a stochastic distribution, which only displays a slight diffusion over time as observed in the projections of the average pixel intensity distributions along the axes. On the other hand, the projections for nanomotors in urea depict a clear anisotropic distribution of the nanomotors, evidenced by the dynamic changes in the projections (Figure 3b). Next, to have a better description of the collective behavior of the swarm, we performed a computational analysis of the evolution of the swarm's effective area (see Movie S3 in the Supporting Information). As can be seen in Figure 3c, in the absence of fuel, motors simply diffuse from the seeding point, and this can be appreciated as a continuous increase in the effective area occupied by the swarm cloud as a function of time (expansion). This is further supported by comparing the frames of the color-coded videos at time points 0 and 120 s, where the decrease in pixel intensity reflects the concentration and therefore the diffusion of the nanomotors from the seeding point. When urea is present, the collective behavior emerges, and the evolution of the effective cloud area becomes more complex (Figure 3d). In the case of the swarm analyzed in this figure, three regimes of movement can be observed: the expansion of the swarm cloud at early time points (1); the formation of plums (2); and the further displacement and expansion of the plums (3). The formation of the plums is depicted as a decrease of the effective area occupied by the swarm cloud, as can be clearly appreciated in the insets of Figure 3d, at 20 and 80 s and the snapshots depicting the pixel intensity at different selected time point (0, 20, 80, and 120 s), where the increase in the pixel intensity reflects the concentration of motors in these unstable fronts. This emergent collective behavior leading to the formation of plums was observed in every case for IONP motors in the presence of urea as can be seen in Figure S2 for another example of an IONP swarm. Moreover, this type of emerging phenomenon was also reported in a previous study from our group for swarms of mesoporous silica urease-based motors.[37]

Light-Triggered Collagen Fiber Disruption by IONP Motors. In the previous section both enhanced diffusion of single IONP motors and collective swarming behavior in the presence of urea as fuel were observed. The next step was to evaluate the capability of the IONP NMs to form VNBs upon nanosecond laser irradiation. Formation of VNB can be conveniently visualized by dark-field microscopy (Figure 4ai).[45,46] As can be seen in the graph in Figure 4aii, the number of VNBs within the illuminated laser area (7 ns laser pulse, λ = 561 nm) gradually increased with increasing laser fluence, until all particles in the irradiated area formed VNBs. From such a graph, the VNB threshold can be derived, which is commonly defined as the laser fluence at which 90% of the particles form VNBs.[46] After fitting of a Boltzmann function, the VNB threshold was found to be 0.97 J/cm^2.

Having confirmed VNB formation by IONP NMs, the next step was to confirm if this allows a biological barrier model to be disrupted that shields cells from nanocarriers (Figure 4aiii). One of the most extensively explored biological barriers is the extracellular matrix (ECM), as it is known that tumors often possess a denser extracellular matrix that prevents adequate nanocarrier penetration, leading to suboptimal therapeutic efficiencies.[2] The ECM is a hydrated polymer network mainly composed of two categories of molecules: proteoglycans, and fibrous proteins, such as collagen and fibronectin. Moreover, elongated fibers based on collagen glycoproteins are one of the main components that provide structural support to the EMC of connective tissues.[47] Collagen fibers were created by heating type I collagen solutions, as previously described.[31] As shown in Figure 4bi, collagen solution turbidity (measured at λ = 400 nm) increased over time upon heating at 37 °C, indicating the formation of collagen fibers (see inset images at the initial time point and after 24 h). The presence of collagen fibers was further confirmed by dark-field microscopy (Figure 4bii).

We analyzed VNB-mediated collagen fiber disruption at the single fiber level. First, a dispersion of fibers (0.2 mg/mL) was incubated for 1 h with IONP motors (0.01 mg/mL) in the presence of urea (300 mM) in PBS. Figure 4c shows representative dark-field images before (i), during (ii), and after irradiation with one (iii) and five (iv) laser pulses at the VNB threshold (0.97 J/cm^2, 7 ns laser pulse, λ = 561 nm). Vapor nanobubbles could be clearly observed arising from IONP motors attached to the fibers (highlighted with yellow arrows in Figure 4cii). One laser pulse was sufficient to fragment the fiber, becoming completely disrupted after 5 pulses. The complete irradiation and disruption sequence can be seen in the Supporting Information (Movie S4). After this successful first result, we proceeded to perform bulk measurements by quantifying the rheological properties of a collagen fiber dispersion. For this, we determined the viscosity, storage G' and loss G'' modulus as a function of the shear rate of a dispersion of collagen fibers (0.2 mg/mL) incubated for 1 h with IONP motors (0.01 mg/mL) in the presence of 300 mM urea in PBS (see Supporting Information Figure S3a). In particular, we evaluated the effect of the VNB-mediated disruption of the fibers upon irradiation with 1, 5, or 10 pulses at the VNB threshold. Controls included collagen fibers, fibers co-incubated with IONP motors without fuel, and fibers after

https://doi.org/10.1021/acsnano.2c09380
ACS Nano 2023, 17, 7180−7193

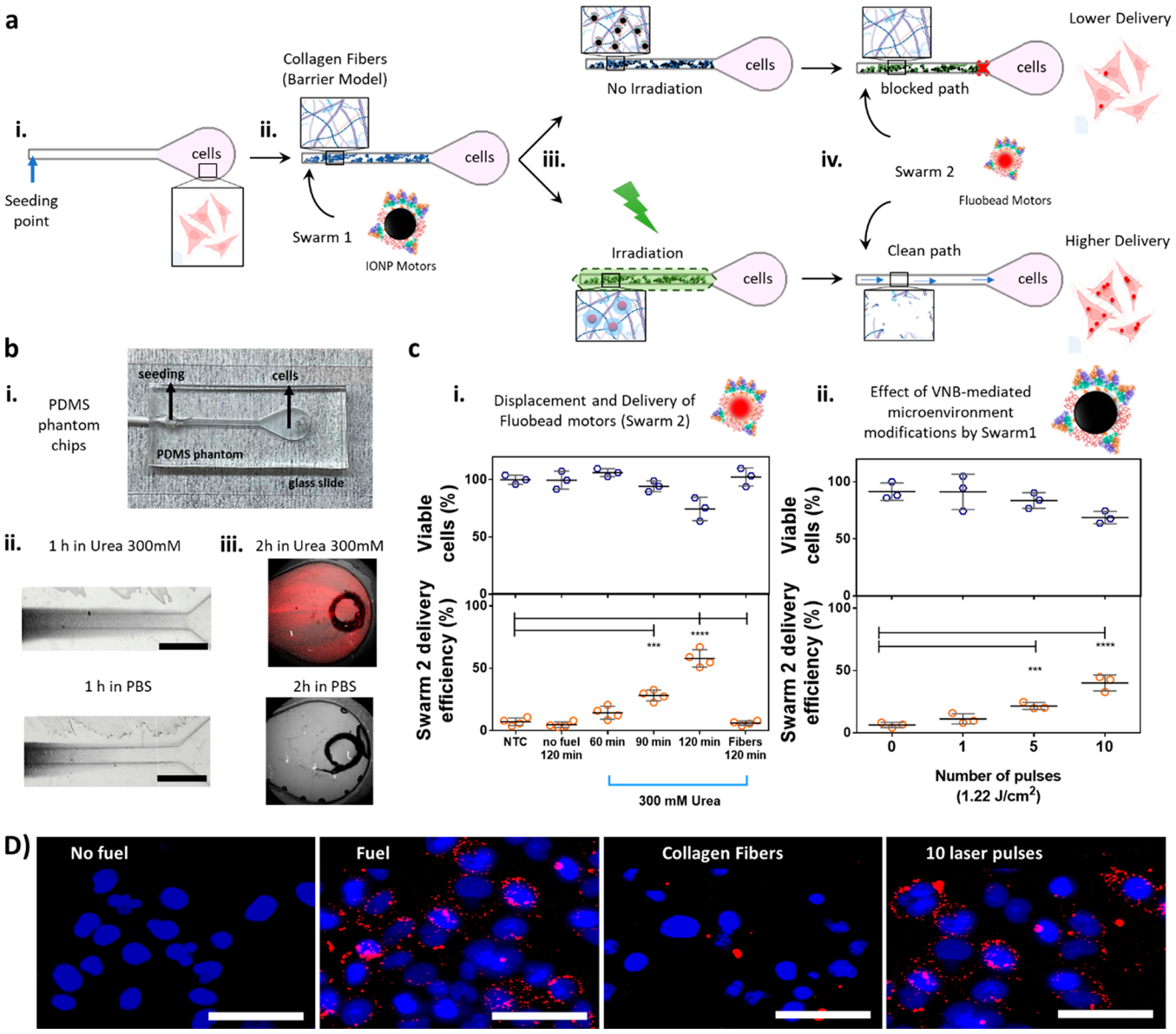

Figure 5. Evaluation of swarms of nanomotors as delivery strategy in phantom lab-on-a-chip to HeLa cells. (a) Schematic overview of the experimental design: (i) Phantom chip containing a reservoir with HeLa cells. (ii) The chip's channel was first filled with collagen fibers dispersed with 300 mM urea in PBS, prior the addition of Swarm 1. (iii) After incubation, the channels were irradiated with 0, 1, 5, or 10 laser pulses (1.22 J/cm^2, 5 ns, λ = 532 nm). The induced mechanical damage disrupts the collagen fibers generating a clean path for Swarm 2. (iv) Swarm 2 is added. (b) PDMS phantom chips. (i) Scheme depicting the fabricated chips. Collective displacement of (ii) IONP motors after 1 h and (iii) Fluobead motors after 2 h of being added at the seeding point in channels filled with 300 mM urea in PBS or just PBS (control). (c,i) Delivery efficiency of Swarm 2 in HeLa cells as a function of the time after seeding of the motors. Controls include the quantification of the delivery efficiency 120 min after seeding of the Fluobead motors in channels filled just with PBS and channel filled with collagen fibers dispersed in 300 mM urea in PBS. (ii) Evaluation of the two-swarms delivery strategy described in panel (a). Swarm 1 was incubated 1 h, prior irradiation with different number of pulses (0, 1, 5, or 10 pulses with a fluence of 1.22 J/cm^2, 5 ns, λ = 532 nm). After the irradiation, Swarm 2 was added and incubated for 120 min. Cell viability was determined for all experiments by a CellTiter-Glo assay postdelivery. Statistical significance (one-way ANOVA) is indicated when appropriate (*p < 0.05, **p < 0.01, ***p < 0.001, ****p < 0.0001). (d) Representative microscopy images of HeLa cells after treatment for different conditions: Fluobead motors incubated 120 min in the absence of urea (no fuel); Fluobead motors incubated 120 min with 300 mM urea in PBS in the presence (collagen fibers) or absence of collagen fibers (fuel); Fluobead motors incubated 120 min after treatment with IONP motors and 10 pulses irradiation (10 laser pulses). Scale bar represents 30 μm.

tip sonication (20%, 20 s) as a positive control of total fiber disruption. From the obtained graphs, we selected a defined shear rate to compare between the different experimental conditions. The quantification of the rheometry measurements of (i) the viscosity at a shear rate of 100 (1/s) and (ii) the storage G' and loss G'' modulus at a shear rate of 0.1 (1/s) are shown in Figure 4di,ii, respectively. Viscosity measurements revealed no significant changes when fibers were incubated with NMs in the absence of fuel. In the presence of fuel, the enzymatic catalysis induced a significant 49.1 ± 0.5% reduction of the viscosity after 1 h. This partial chemical degradation of the collagen fibers was further enhanced by irradiation at the

https://doi.org/10.1021/acsnano.2c09380
ACS Nano 2023, 17, 7180−7193

VNB threshold, which showed a consistent decrease in the viscosity as a function of the number of laser pulses applied, reducing the viscosity by 88.2 ± 0.3% after 10 pulses. This drastic decrease in the bulk viscosity is equivalent as observed for the positive control (90.7 ± 0.3% reduction). Afterward, we proceeded to characterize the storage modulus (G') and the loss modulus (G'') of the samples (Figure 4dii), which relative intensities and absolute values are related to the viscoelastic character and the strength of the fibrous network. Hand in hand with the observed decrease in viscosity, there is a clear decrease in the storage and loss moduli for samples treated with IONP motors in the presence of urea in comparison to fibers alone and the control experiment using motors in absence of fuel. These observations reinforce the hypothesis of a partial degradation induced by the enzymatic reaction. Previous reports have shown that the pH changes induced by the products of the urease-urea reaction can induce degradation of mucin matrices, reducing its viscosity.[19] To further elucidate if the pH change induced by the enzymatic reaction could lead to the degradation of the collagen fibers, we first quantified the pH change after 1h incubation of the IONP motors in the presence of 300 mM urea in PBS (initial pH = 7.5; final pH = 10.5), as shown in Figure S3bi. Next, we incubated the collagen fibers for 1h in PBS at the adjusted pH before performing the rheological measurements. As can be seen in Figure S3bii in the Supporting Information, after 1 h incubation at pH = 10.5 the rheological properties depict a clear decrease of the viscosity in the whole shear rate range. Note that the differences in viscosity observed by 1 h incubation at the adjusted pH are more drastic than those observed for 1 h incubation in the presence of motors and 300 mM urea in PBS (Figure S3ai), as in this last case, the pH is a consequence of the enzymatic reaction which generates progressive changes in the pH until reaching a pH = 10.5. Overall, these experiments corroborated that the use of urease-powered motors can per se improve the capability of passive nanocarriers to degrade biological barriers. Nevertheless, the results in Figure 4dii clearly indicate that chemical degradation alone can only induce a partial degradation of the collagen fibers. After applying 10 laser pulses, G' and G'' reduced to similar levels as for the tip sonication positive control, showing that laser-induced VNB are able to completely degrade the fibers (Figure 4diii). This is in line with previous reports in which collagen fibers and vitreous opacities ("eye floaters") could be destroyed by VNBs when using gold nanoparticles as photothermal nanoparticles.[31,48]

Evaluation of Swarms of Nanomotors As a Delivery Strategy for Overcoming Extracellular Barriers. Scientists in the nanorobotics field have started to explore the combination of surface modification with added capabilities, among which light-triggered photothermal effects for barrier degradation are on the leading edge.[49] Despite their relative success, many of these strategies only offer partial degradation and fail to adequately address the barriers. In the previous section, we demonstrated that, under certain irradiation conditions (typically using ns laser pulses),[50] photothermal properties of the NMs can be used to induce the formation of VNBs that can mechanically disrupt the biological barriers instead of inducing heat-mediated degradation.

To evaluate if the microenvironment modifications would improve the delivery efficiency of another swarm of motors, we designed a model motor based on fluorescent beads (Fluobead motors), allowing for an easy read-out of the delivery to the cells by flow cytometry, named Swarm 2. The rationale behind the separation of the disruptive effect and the delivery into two different swarms is linked to the possible degradation of the cargo in nanocarriers that can per se form VNBs upon laser activation, as previously reported for the degradation of pDNA in polyplexes containing gold nanoparticle clusters after VNB formation.[51] This is not restrictive for nucleic acids, but also for enzymes, as demonstrated by the disappearance of the urease activity of IONP motors after irradiation (see Figure S4 in the Supporting Information). For the synthesis of Swarm 2, we made use of PEI-coated 200 nm polystyrene beads, which were further chemically functionalized using glutaraldehyde for the click chemistry binding of urease in the presence of amino-PEG as stabilizer (Figure S5ai in the Supporting Information). The physicochemical characterization by DLS and zeta-potential measurements during the different functionalization steps, and the enzymatic activity of the final Fluobead motors can be found in Figure S5aii–iv in the Supporting Information, respectively. Similarly, as for IONP motors (Figure 2c,d), the motion analysis of the urease-powered Fluobead motors also depicted a significant increase in the diffusion coefficient dependent on urea concentration, reaching a maximum of 1.2 ± 0.1 $\mu m^2/s$ at 300 mM of urea (Figure S5b in the Supporting Information). In addition, as shown in Figure S5c, Fluobead motors presented in vitro swarming behavior in the presence of fuel, adding further evidence that urease-powered NMs can form swarms when swimming without boundaries despite the composition of the motor chassis (Movie S5).

To evaluate the possible added value of the collective effects of swarms of NMs, we designed phantom chips in which the NMs are seeded at one end of a microchannel leading to a reservoir containing HeLa cells (often-used model cell line for delivery studies). Delivery efficiency was quantified by flow cytometry, while cell viability was determined in parallel using the CellTiter-Glo metabolic assay. Figure 5a shows a schematic overview of these experiments: (i) HeLa cells (15000 cells) were seeded and cultured for 24 h before the experiments. (ii) The chip's channel was filled with collagen fibers (0.2 mg/mL) dispersed in 300 mM urea in PBS, prior to addition of Swarm 1 of IONP motors (0.01 mg). (iii) After a certain incubation time, the channels were irradiated with 0, 1, 5, or 10 laser pulses (1.22 J/cm^2, 5 ns, λ = 532 nm) to induce mechanical damage due to the VNB formation and collapse. Note that for these experiments we made use of a dedicated home-built setup with a nanosecond pulsed laser (5 ns pulse duration, 532 nm wavelength) that allows fast scanning of the laser beam. The required irradiation fluence on this setup for the induction of VNBs from the IONPs was previously determined to be 0.84 J/cm^2.[39] We proceeded to irradiate at 1.22 J/cm^2 to ensure to be in the VNB regime to maximize the mechanical damage exerted by the collapsing bubbles. (iv) This second swarm of Fluobead motors was added (0.016 mg) and incubated prior to cell trypsinization and flow cytometry analysis.

Regarding the lab-on-a-chip fabrication, polydimethylsiloxane (PDMS) channels were fabricated, which were further attached to a glass slide by plasma cleaning (Figure S6a). The parameters of the fabricated chips can be found in Figure S6b in the Supporting Information. Two access sites were foreseen in the lab-on-a-chip devices, one at the reservoir region to allow cell seeding and one on the other side of the microchannel to insert the different swarms of NMs (Figure 5bi). We started by evaluating the displacement of Swarm 1

https://doi.org/10.1021/acsnano.2c09380
ACS Nano 2023, 17, 7180−7193

with IONP motors in the presence and absence of 300 mM urea in PBS. Active motors were able to spread along the whole channel after 1 h incubation, while the passive particles simply got deposited at the seeding point (Figure 5bii). The selected incubation time for Swarm 1 was applied for the rest of the experiments, as these motors will only need to be present in the channel where the collagen fibers will be placed (Figure 5aii). This is not the case for Swarm 2, which needs to reach the cells in the reservoir. In that sense, Figure 5biii shows representative images demonstrating the arrival of Swarm 2 and its distribution along the whole reservoir after 2 h seeding (maximum incubation time point for Swarm 2). We proceeded to quantify the delivery efficiency of Swarm 2 in precultured HeLa cells (Figure 5ci). We started by evaluating the delivery efficiency in absence of the biological barrier (collagen fibers) to determine the maximum efficiencies possible for Swarm 2. An increasing trend for the delivery efficiency is observed as a function of the incubation time in the presence of fuel (300 mM urea in PBS), which becomes significant compared to nontreated cells after 90 min and reaching a maximum of 58% positive cells 120 min after seeding. Note that no significant increase in the delivery efficiency could be obtained in the absence of fuel or in the presence of collagen fibers blocking the channel, even after 120 min. This result clearly indicates that the swarming behavior of the active particles is needed to induce the collective displacement of the Fluobead motors toward the cells region in the lab-on-a-chip platform. Cell viability was measured in parallel, indicating a decreasing trend as a function of time after seeding the NMs, reaching a viability of 75% after 120 min. This decrease in the cell viability can be linked to an increase in NM uptake and the presence of byproducts from the enzymatic reaction, especially ammonia, which induces pH changes.[8]

The results indicate that the collagen fibers in the channel act as a real barrier preventing Swarm 2 to reach the cells. We proceeded to test if VNB generation by Swarm 1 would induce an enhancement in the delivery of subsequently added Swarm 2 (sequential treatment of swarms). For this, we followed the experimental scheme presented in Figure 5a, making use of the optimized incubation times for Swarm 1 (1 h) and Swarm 2 (2 h). Figure 5cii shows the obtained delivery efficiencies of the Fluobead motors and cell viabilities as a function of the number of laser pulses. An increasing trend in the delivery efficiency was observed as the number of laser pulses increased, reaching 21 and 40% positive cells for 5 and 10 pulses, respectively. This result (40% positive cells) represents a 10-fold enhancement of the delivery efficiency in comparison with nonirradiated samples and indicates that the fibers were successfully disrupted by Swarm 1. These results were further confirmed by light microscopy, as depicted from the detection of the Fluobead motors (red) in cells imaged 120 min after seeding of the motors in the absence of collagen fibers in the presence of fuel (label "fuel"), as well as in the presence of collagen fibers but after applying the treatment with Swarm 1 and irradiation with 10 pulses (label "10 laser pulses"). The corresponding controls with Fluobead motors in the absence of fuel (label "no fuel"), or in the presence of fuel and collagen fibers (label "collagen fibers"), showed clearly lower numbers of particles of Swarm 2. As urea is well-known to affect the stability of proteins,[52] we also performed experiments in which the concentration of urea remained constant by making use of particles without urease (passive particles). Figure S7a in the Supporting Information show the effect on the viscosity of a dispersion of collagen fibers incubated for 1 h in the presence and absence of 300 mM urea in PBS, where it can be appreciated a decrease in the overall viscosity. Despite the observed urea-mediated fibers degradation, we did not observe any effect in the delivery toward cells following the two-troops treatment using nanoparticles without urease in the presence of 300 mM urea in PBS (see Figure S7b in the Supporting Information). This results clearly indicate that despite urea can induce denaturation of the protein fibers this denaturation alone is not sufficient to allow proper delivery by passive diffusion of the nanoparticles. The presence of the enzymes and the fuel are both equally important to generate the swarming effects responsible of the active collective displacement of particles.

Additionally, we proceeded to evaluate the effect of the coadministration of Swarm 1 and Swarm 2 prior irradiation (See Figure S8 in the Supporting Information). Despite an increasing trend in the delivery as a function of the number of laser pulses was observed, similarly as in the case of the sequential administration strategy, the results obtained by the coadministration strategy (28% of positive cells for 10 pulses) lay below the obtained for the sequential administration (40% of positive cells for 10 pulses). To put the results in perspective, we calculated the percentages of delivery efficiency of Fluobead motors (Swarm 2) normalized to the maximum delivery obtained (58% of positive cells) for the clean path condition (absence of protein aggregates in the channel), which was assigned to 100%. The results presented in Figure S9 in the Supporting Information, include the condition of blocked path (presence of fibers) for comparison, which account for only 6% of the maximum delivery achieved, and the coadministration (48%) and sequential administration (71%) of Swarm 1 and Swarm 2, in combination with 10 pulses irradiation. These results indicate that the overall delivery benefits from the separation of the process into a first VNB-mediated microenvironment modification to clean the path for the addition of Swarm 2 in a second stage. A possible explanation of the lower delivery efficiency obtained with the coadministration strategy could be linked to the lack of control of the different fluid phenomena generated upon VNB formation and collapse. In this regard, the shockwaves generated for the disruption of the fibers are being induced without any preferential orientation while the Fluobead motors collectively displace toward the cells, which could lead to perturbation in their collective displacement.

CONCLUSION

In summary, we have shown that the design of a nanomotor that, in addition to self-propulsion and swarm formation, generates VNBs upon nanosecond pulsed-laser irradiation, allowing mechanical damage on the surrounding microenvironment. Such effect was demonstrated by completely disrupting collagen fibers in a lab-on-a-chip system. The collective swarming behavior of these enzyme-powered motors (Swarm 1) was exploited to displace and accumulate in the channels filled with collagen fibers (acting as a barrier model of the ECM). We found that, upon laser treatment, the disruption of the barrier blocking the channels permitted the active transport of swarms of nanomotors acting as a reporter (Swarm 2) toward cells, showing a 10-fold enhancement in the delivery efficiency. The approach here described, based on the use of different swarms of nanomotors with advanced photothermal effects for trespassing biological barriers (overcoming passive

https://doi.org/10.1021/acsnano.2c09380
ACS Nano 2023, 17, 7180−7193

diffusion and steric hindrance limitations), denotes a clear potential therapeutic application. Future work using drug-loaded motors as Swarm 2 needs to be addressed to evaluate effective intracellular delivery and its biological effect in more realistic in vitro and ex vivo scenarios, where the already advantageous effect of self-propulsion can be combined with the disruptive therapeutic capabilities of VNBs.

MATERIALS AND METHODS

Materials. Mono Mag magnetic beads 0.5 μm (Ocean NanoTech), glutaraldehyde grade II (Glu, 25% in H_2O), HS-PEG5K-NH_2 (HCl salt), urease (from *Canavalia ensiformis*, Type IX, powder, 50 000−100 000 units g/g solid), urease activity kit, urea (99.9%), and urease (from *Canavalia ensiformis*, Type IX, powder, 50 000−100 000 units/g solid) were obtained from Sigma-Aldrich. Red fluorescent amine-modified beads 0.2 μm (2% solids), PBS, Pierce BCA protein assay kit, and Dulbecco's modified Eagle's medium (DMEM) were purchased from ThermoFischer Scientific. Standard gray V4 resin (FLGPGR04) for the 3D printing of rigid molds was purchased at FormLabs.

NM Synthesis and Characterization. IONP motors were synthesized using 0.5 μm amine Mono Mag magnetic beads (Ocean NanoTech, USA), named "IONPs" in the article, which consist of a polymeric NP coated with iron oxide. Briefly, IONPs (2.5 mg) were suspended in PBS (1×), and 10 μL of Glu (2.5% in water) was added to mixture (final volume = 0.5 mL). The mixture was thoroughly vortexed to ensure good dispersion and shaken for 2 h to obtain glutaraldehyde-functionalized IONPs (IONP@Glu). Then the particles were collected by centrifugation (3 min, 1900 rcf) and washed 2 times with PBS. Next, IONP@Glu was suspended in 50 μL of HS-PEG5K-NH_2 (0.04 mg/mL) and vortexed for 1 min prior to addition of 450 μL of PBS containing urease (final urease concentration = 6 mg/mL) and mixed for 24 h in an end-to-end on a rotary shaker. The resulting IONP motors were collected by centrifugation (3 min, 1900 rcf) and washed 2 times with PBS.

The synthesis of Fluobead motors was performed following the same protocol described above for IONP motors but starting from 4 mg of 200 nm fluorescent particles and performing the washing steps by centrifugation for 5 min at 9300 rcf.

For the physicochemical characterization, NMs were washed and resuspended in MQ water, after which they were transferred either into a disposable folded capillary cell (Malvern, Worcestershire, UK) or into a disposable cuvette (Brand, Wertheim, Germany) for further measurement of their zeta-potential or hydrodynamic size, respectively, using a Malvern Zetasizer Nano (Malvern Instruments Ltd., Worcestershire, UK). The measurements were performed in triplicate at a temperature of 25 °C.

The activity of the covalently bound urease and the total protein content of the supernatants of the washing steps and the final motors were evaluated using a commercial urease activity kit and total protein assay, respectively, following the manufacturer's instructions.

Motion and Tn Vitro Swarming Analysis. Observation and video recording of the NMs was performed in an inverted optical microscope (Leica DMi8) using a 63× water objective. Briefly, 5 μL of NMs in PBS were placed on the center of a 9 mm diameter and 0.12 mm deep Secure-Seal spacer (ThermoFischer Scientific) sticked onto a glass slide and thoroughly mixed with the solutions of urea in PBS at the desired concentrations. Then, the mixture was covered using a coverslip to avoid artifacts caused by the drifting effect. Videos of 30 s were recorded using a Hamamatsu camera at a frame rate of 50 fps, under bright field. The analysis of motion was performed with the Python-based Nanomicromotor Analysis Tool (NMAT) v. X (https://github.com/rafamestre/NMAT-nanomicromotor-analysis-tool) to obtain the tracking trajectories, MSD, and diffusion coefficients as previously described.[53] The resulting MSD and diffusion coefficients were obtained by analyzing a minimum of 15 particles per condition and the error represents SE.

The optical videos of the swarms of NMs were acquired using a THUNDER Leica microscope, using a 2.5× objective. For this, a 2 μL droplet of NMs (5 mg/mL) suspended in PBS was placed in the middle plane of a 3 mL Petri dish containing either PBS (control) or a solution of 300 mM urea in PBS, and 2 min videos were acquired at a frame rate of 25 frames per second as previously reported.[37]

For the computational analysis (i.e., the calculation of the projections and the effective area of the NM swarm), the background was subtracted from each frame of the video. As a background image, the first frame was taken in which the area occupied by the cloud was replaced by a mean value of the vicinity. First, the projections are calculated as the sum of all pixel intensities along x:

$$\bar{I}_{\mathrm{proj}}(y) = \frac{1}{N_x}\sum_{n=1}^{N_x} I_n(y) \tag{1}$$

where N_x denote the width of the image in pixels. The projections along y-axis are being calculated accordingly with N_y being the height of the image. Equation 1 refers to the projection of one image and is therefore performed for all frames of the videos accordingly. Note that the image intensities I are normalized and range between 0 and 1. Then an intensity threshold of 10% of the global maximum intensity value was used for the control and the 300 mM samples. Pixels of intensity values above this threshold are considered as effective area occupied by the NM swarm. Using this threshold, the images of the video are converted into a binary image using

$$I^{\mathrm{bi}} = \begin{cases} 1 \text{ for } I \geq 0.1\, I_{\max} \\ 0 \text{ else} \end{cases} \tag{2}$$

The effective area is then calculated as the sum of the binary pixel intensities:

$$A = \sum_{n=1}^{N} I^{\mathrm{bi}}(x, y) \tag{3}$$

where $N = N_x N_y$ being the total number of pixels.

Formation of Collagen Fibers as a Model for Extracellular Barriers. Collagen I from rat tail was dissolved in PBS (0.2 mg/mL), and the pH of the collagen solution was increased to 7−8 with NaOH (0.1 N). Subsequently, the collagen solution was incubated at 37 °C for 1 h to obtain the artificial opacities visible by eye, which were further stored at 4 °C. To follow the fibrillation process, turbidity experiments were performed by measuring the absorbance of the collagen suspension (λ = 400 nm) at 37 °C (using a NanoDrop 2000c spectrophotometer). Formation of collagen fibers was further confirmed by confocal microcopy making use of a dark-field condenser.

VNB Generation Threshold and Single Collagen Fiber Disruption upon Irradiation of IONP Motors. An in-house developed optical setup was used to determine the laser pulse fluence threshold, which is defined as the laser fluence of a single laser pulse at which 90% of the irradiated NPs generate a VNB.[54] In short, IONPs (stock: ~1.3 × 10^9 NPs/mL) were first diluted 100× in PBS and transferred to a 50 mm γ-irradiated glass-bottom dish (MatTek Corporation, Ashland, MA, USA). After sedimentation of the NPs, the samples were mounted on an inverted microscope (TE2000, Nikon BeLux, Brussels, Belgium) and irradiated with a pulsed laser (7 ns) tuned at a wavelength of 561 nm (Opolette HE 355 LD, OPOTEK Inc., Carlsbad, CA, USA). The laser beam diameter at the sample was 150 μm. The laser pulse energy was monitored using an energy meter (LE, Energy Max-USB/RS sensors, Coherent). An electronic pulse generator (BNC575, Berkeley Nucleonics Corporation), synchronized with an EMCCD camera (Cascade II: 512, Photometrics), was used to trigger individual laser pulses and record dark-field microscopy images before, during, and after VNB formation. VNBs can be seen distinctly in dark-field microscopy images as brief bright localized flashes of light due to the increased light scattering during their lifetime. By quantifying the number of visible VNBs within the laser pulse area (150 μm diameter) for increased laser pulse fluences, the VNB generation threshold can be determined. This setup was also used for visualization and disruption of individual collagen fibers after irradiation at the VNB threshold fluence (0.97 J/cm^2). For this experiment, 1 mL of collagen fibers (0.2

https://doi.org/10.1021/acsnano.2c09380
ACS Nano 2023, 17, 7180−7193

mg/mL) were centrifuged and resuspended in 300 mM urea in PBS and incubated with IONP motors (0.01 mg/mL) for 1 h. After this incubation time, the system was diluted 1000× and transferred to a 50 mm γ-irradiated glass-bottom dish.

Images were analyzed using the ImageJ software (FIJI, https:/Fiji.sc/) to visualize and quantify the number of VNBs and the disruption of the collagen fibers.

Rheological Measurements. The rheological characterization of collagen fibers dispersions with or without the different treatments were performed using an Anton Paar MCR 702 rheometer, with a cone-and-plate geometry of 1.005° and 40 mm in diameter. Temperature was controlled within ±0.2 °C during measurements at 25 °C. All rheological measurements were performed at least three times, reporting the average values. Viscosity, storage G', and loss G'' modulus were measured by using a minimum volume of 400 μL per each sample, being determined as a function of the share rate from 0.1 to 100 s^{-1}. Briefly, samples of 1.5 mL of collagen fibers (0.2 mg/mL) were incubated for 1 h with IONP motors (0.01 mg) in the presence of 300 mM urea in PBS, prior to irradiation with 0, 1, 5, or 10 pulses at the VNB threshold. For the irradiation, samples were transferred just after 1 h incubation to 50 mm γ-irradiated glass-bottom dishes. Controls included collagen fibers alone, fibers co-incubated 1 h with IONP motors without urea in PBS, and fibers after tip sonication (20%, 20s). The last one as a positive control of total fiber disruption.

PDMS Phantom Chip Fabrication. To analyze the collective displacement and swarming effect of the NMs, lab-on-a-chip systems were fabricated as phantoms composed of a linear channel connected to a funnel-like reservoir on the other extreme, whose total area was 50 mm^2 and which was aimed for cell seeding. The 3D structure from the rigid mold was designed using AutoCAD software and further 3D printed by using stereolithography techniques. The resulting rigid mold containing the inverse design of the desired phantom was printed and processed as previously described.[37] Briefly, the nonpolymerized resin was removed by two sequential washing steps in an isopropanol bath, followed by hardening of the photopolymerized resin by 15 min exposure to ultraviolet light. To fabricate the flexible and transparent polydimethylsiloxane (PDMS)–based structures, the catalyzer and the monomer were first mixed at a ratio of 1:10, and the solution was degassed for 15 min to avoid the presence of bubble in final lab-on-a-chip configuration. The solution was poured onto the rigid mold, degassed for 15 min, and finally cured at 65 °C overnight. The polymerized PDMS was then removed from the rigid mold. To close the system and obtain the final chip, the channel's open side was bound to the glass coverslip by previously exposing both, coverslip and the phantom, to 2 min plasma treatment. Openings were made on top of the reservoir and on the side of the linear channel for cells and NMs seeding, respectively.

The collective NMs displacement in the final phantom chips was evaluated with optical microscopy using a THUNDER Leica microscope. For this, a 2 μL droplet containing 0.01 and 0.016 mg of IONP motors and Fluobead motors, respectively, was seeded in one of the extremes of the phantom chip containing either PBS (control) or a solution of 300 mM urea in PBS.

Cell Culture. HeLa cells (cervical adenocarcinoma cells, ATCC CCL-2) were cultured in Dulbecco's modified Eagle's medium containing growth factor F-12 (DMEM/F-12). Full cell medium was prepared by adding 10% FBS, 2 mM L-glutamine, and 100 μg/mL penicillin/streptomycin as supplements. Cells were seeded at a density of 15^4 cells/well in the PDMS reservoir and incubated for 24 h at 37 °C, 5% CO_2 prior treatment.

Evaluation of Swarms of Nanomotors as Delivery Strategy in Phantom Chips to HeLa Cells. HeLa cells were seeded (15000 cells) 24h every delivery experiments. A typical delivery experiment with the Fluobead motors (Swarm 2) consisted in filling the chip's channel with 300 mM urea in PBS or simply PBS, prior seeding 2 μL containing 0.016 mg of NMs at the opposite extreme of the cell's reservoir. After a certain incubation time (60, 90, or 120 min), cells were trypsinized and resuspended in flow buffer prior analysis by flow cytometry. The biological barrier effect was evaluated by filling the chip's channel with collagen fibers (0.2 mg/mL) in 300 nM urea in PBS, prior the seeding and incubation for 120 min of Fluobead motors.

The disruption of the biological barrier model was evaluated by the two-swarms strategy. For the sequential administration strategy, the channel from the lab-on-a-chip platform was first filled with collagen fibers (0.2 mg/mL) dispersed in urea (300 mM) in PBS, prior addition of 2 μL of Swarm 1 of IONP motors (containing 0.01 mg IONP motors). After 1 h incubation, the channels were irradiated with 1, 5, or 10 laser pulses (1.22 J/cm^2, 5 ns, λ = 532 nm), avoiding the irradiation exposure to the reservoirs containing cells. Next, 2 μL containing 0.016 mg of Swarm 2 of Fluobead motors was seeded and incubated for 120 min prior trypsinization for flow cytometry measurements. For the coadministration strategy, 4 μL was added containing 0.01 mg of IONP motors (Swarm 1) and 0.016 mg of Fluobead motors (Swarm 2). After 1 h, the channels were irradiated with 0, 1, 5, or 10 laser pulses. The system was left for 1 h more to proceed (total time = 120 min) prior to trypsinization for flow cytometry measurements.

Viability was assessed after treatment using the CellTiter-Glo luminescent cell viability assay, as recommended by the manufacturer (Promega, Leiden, The Netherlands). Briefly, HeLa cells were recovered from the lab-on-a-chip's reservoir by trypsinization and further neutralized with full cell medium before being transferred to a 96-well plate. They were supplemented with an equal volume of CellTiter-Glo reagent for each well (50 μL), mixed for 5–10 min using an orbital shaker (120 rpm), and transferred to an opaque 96-well plate. After allowing the plate to stabilize for 10 min, the luminescent signal of each well was measured using a Glomax luminometer (Promega, Leiden, The Netherlands).

For the Fluobead motors delivery visualization, instead of being trypsinized as in the flow cytometry measurements, cells were directly imaged in the phantom lab-on-a-chip after treatment by optical microscopy (Leica DMi8). Cells were first incubated with Hoechst33342 (1000×) for 10 min at 37 °C. After staining, the cells were washed with culture medium and imaged using confocal microscopy. Images were analyzed using the NIS-Elements Viewer 4.20 software.

Flow Cytometry. Quantifications based in fluorescence were performed using a CytoFLEX flow cytometer (Beckman Coulter, Suarlée Belgium). The resulting flow cytometry data were analyzed using FlowJo (Treestar Inc., Ashland, USA) software.

Statistical Analysis. All data are shown as mean ± standard deviation. Statistical differences were analyzed using the Graphpad Prism 8 software (La Jolla, CA, USA). The statistical tests used in each figure are mentioned in the figure caption. Statistical differences with a p value <0.05 were considered significant.

ASSOCIATED CONTENT

Supporting Information

The Supporting Information is available free of charge at https://pubs.acs.org/doi/10.1021/acsnano.2c09380.

Figures showing urease functionalization for IONP motor synthesis, computational analysis of the evolution of swarm's effective area, bulk measurements of collagen fibers' disruption of enzymatic activity, study of the chemical degradation related to the pH change induced by the enzymatic reaction, effect of the number of laser pulses on the enzymatic activity of IONP motors, synthesis and characterization of the urease-powered 200 nm fluorescent polystyrene motors (Fluobead motors), lab-on-a-chip fabrication of phantom chips, evaluation of urea-mediated denaturation of protein aggregates, evaluation of coadministration strategy of Swarm 1 and Swarm 2, and the normalized delivery efficiency percentages (PDF)

Swarming behavior of IONP motors in the presence and absence of 300 mM urea in PBS (AVI)

https://doi.org/10.1021/acsnano.2c09380
ACS Nano 2023, 17, 7180–7193

Evolution of the projections along the axes of the average pixel intensity of IONP motors in the presence and absence of 300 mM urea in PBS (AVI)

Computational analysis of the effective area and pixel intensity of swarms of IONP motors in the presence and absence of 300 mM urea in PBS (AVI)

Disruption by VNB formation upon irradiation of a single collagen fiber after 1 h incubation with IONP motors (AVI)

Swarming behavior of Fluobead motors in the presence and absence of 300 mM urea in PBS (AVI)

AUTHOR INFORMATION

Corresponding Authors

Juan C. Fraire − *Institute for Bioengineering of Catalonia (IBEC), Barcelona Institute of Science and Technology (BIST), 08028 Barcelona, Spain; Laboratory for General Biochemistry and Physical Pharmacy, Faculty of Pharmaceutical Sciences, Ghent University, 9000 Ghent, Belgium;* orcid.org/0000-0002-4887-2161; Email: jfraire@ibecbarcelona.eu

Kevin Braeckmans − *Laboratory for General Biochemistry and Physical Pharmacy, Faculty of Pharmaceutical Sciences, Ghent University, 9000 Ghent, Belgium;* orcid.org/0000-0002-7993-6295; Email: kevin.braeckmans@ugent.be

Samuel Sánchez − *Institute for Bioengineering of Catalonia (IBEC), Barcelona Institute of Science and Technology (BIST), 08028 Barcelona, Spain; Catalan Institute for Research and Advanced Studies (ICREA), 08010 Barcelona, Spain;* orcid.org/0000-0002-5845-8941; Email: ssanchez@ibecbarcelona.eu

Authors

Maria Guix − *Institute for Bioengineering of Catalonia (IBEC), Barcelona Institute of Science and Technology (BIST), 08028 Barcelona, Spain; Departament de Ciéncia dels Materials i Química Física, Institut de Química Teòrica i Computacional Barcelona, Universitat de Barcelona, 08028 Barcelona, Spain*

Ana C. Hortelao − *Institute for Bioengineering of Catalonia (IBEC), Barcelona Institute of Science and Technology (BIST), 08028 Barcelona, Spain*

Noelia Ruiz-González − *Institute for Bioengineering of Catalonia (IBEC), Barcelona Institute of Science and Technology (BIST), 08028 Barcelona, Spain*

Anna C. Bakenecker − *Institute for Bioengineering of Catalonia (IBEC), Barcelona Institute of Science and Technology (BIST), 08028 Barcelona, Spain*

Pouria Ramezani − *Laboratory for General Biochemistry and Physical Pharmacy, Faculty of Pharmaceutical Sciences, Ghent University, 9000 Ghent, Belgium*

Charlotte Hinnekens − *Laboratory for General Biochemistry and Physical Pharmacy, Faculty of Pharmaceutical Sciences, Ghent University, 9000 Ghent, Belgium;* orcid.org/0000-0001-7412-7942

Félix Sauvage − *Laboratory for General Biochemistry and Physical Pharmacy, Faculty of Pharmaceutical Sciences, Ghent University, 9000 Ghent, Belgium;* orcid.org/0000-0002-8065-4439

Stefaan C. De Smedt − *Laboratory for General Biochemistry and Physical Pharmacy, Faculty of Pharmaceutical Sciences, Ghent University, 9000 Ghent, Belgium;* orcid.org/0000-0002-8653-2598

Complete contact information is available at: https://pubs.acs.org/10.1021/acsnano.2c09380

Author Contributions

J.C.F. and S.S. conceived the idea and planned the experiments of this study. J.C.F. performed all the experiments and the data analysis unless specified. M.G. fabricated the PMDS chips and provided guidance for their use. A.C.H. provided overall guidance on the fabrication of the nanomotors, motion analysis and swarming evaluation. A.C.B. performed the computational analysis of the swarms. N.R.G. provided guidance for the rheological measurements. F.S. and P.R. synthesized and characterized the collagen fibers. C.H. participated in the experiments of coadministration of swarms and the evaluation of urease activity after irradiation. J.R. S.S., M.G., K.B. and S.DS. advised on experiments, data analysis, and writing. All authors discussed the experimental results and contributed to writing the manuscript.

Notes

The authors declare no competing financial interest.

ACKNOWLEDGMENTS

This research was funded by European Research Council (ERC) under the European Union's Horizon 2020 research and innovation program (Grant Agreement No. 866348; i-NanoSwarms), "la Caixa" Foundation under the Grant Agreement LCF/PR/HR21/52410022 (BLADDEBOTS project), the CERCA program by the Generalitat de Catalunya, the Secretaria d'Universitats i Recerca del Departament d'Empresa i Coneixement de la Generalitat de Catalunya through the project 2021 SGR 01606, and the "Centro de Excelencia Severo Ochoa", funded by Agencia Estatal de Investigación (CEX2018-000789-S). J.C.F. (FWO grants 1210120N and V407521N), C.H. (FWO grant 1S53521N), and F.S. (FWO grant 12X3222N) gratefully acknowledge The Flemish Research Foundation. J.C.F (2021-BP-00079) and M.G. (2018-BP-00305) acknowledge the Beatriu de Pinós Programme and the Ministry of Business and Knowledge of the Government of Catalonia. M.G. gratefully acknowledge the financial support from the Spanish Ministry of Science through the Ramón y Cajal Grant No. RYC2020- 945030119-I.

ABBREVIATIONS

NPs, nanoparticles; NMs, nanomotors; VNBs, vapor nanobubbles; ECM, extracellular matrix; IONP, iron oxide nanoparticle; Glu, glutaraldehyde; DLS, dynamic light scattering; MSD, mean squared displacement; PDMS, polydimethylsiloxane

REFERENCES

(1) Stewart, M. P.; Langer, R.; Jensen, K. F. Intracellular Delivery by Membrane Disruption: Mechanisms, Strategies, and Concepts. *Chem. Rev.* **2018**, *118*, 7409.

(2) Blanco, E.; Shen, H.; Ferrari, M. Principles of Nanoparticle Design for Overcoming Biological Barriers to Drug Delivery. *Nat. Biotechnol.* **2015**, *33* (9), 941−951.

(3) Rennick, J. J.; Johnston, A. P. R.; Parton, R. G. Key Principles and Methods for Studying the Endocytosis of Biological and Nanoparticle Therapeutics. *Nat. Nanotechnol* **2021**, *16* (3), 266−276.

(4) Arqué, X.; Patiño, T.; Sánchez, S. Enzyme-Powered Micro- and Nano-Motors: Key Parameters for an Application-Oriented Design. *Chem. Sci.* **2022**, *13* (32), 9128−9146.

(5) Gao, W.; Wang, J. Synthetic Micro/Nanomotors in Drug Delivery. *Nanoscale* **2014**, *6* (18), 10486−10494.

(6) Sanchez, S.; Soler, L.; Katuri, J. Chemically Powered Micro- and Nanomotors. *Angewandte Chemie - International Edition* **2015**, *54* (5), 1414−1444.
(7) Mathesh, M.; Sun, J.; Wilson, D. A. Enzyme Catalysis Powered Micro/Nanomotors for Biomedical Applications. *J. Mater. Chem. B* **2020**, *8* (33), 7319−7334.
(8) Hortelão, A. C.; Patiño, T.; Perez-Jiménez, A.; Blanco, À.; Sánchez, S. Enzyme-Powered Nanobots Enhance Anticancer Drug Delivery. *Adv. Funct Mater.* **2018**, *28* (25), 1705086.
(9) Llopis-Lorente, A.; Garciá-Fernández, A.; Murillo-Cremaes, N.; Hortelaõ, A. C.; Patinõ, T.; Villalonga, R.; Sancenón, F.; Martínez-Máñez, R.; Sánchez, S. Enzyme-Powered Gated Mesoporous Silica Nanomotors for on-Command Intracellular Payload Delivery. *ACS Nano* **2019**, *13* (10), 12171−12183.
(10) Hortelão, A. C.; Carrascosa, R.; Murillo-Cremaes, N.; Patiño, T.; Sánchez, S. Targeting 3D Bladder Cancer Spheroids with Urease-Powered Nanomotors. *ACS Nano* **2019**, *13* (1), 429−439.
(11) Peng, F.; Tu, Y.; Men, Y.; van Hest, J. C. M.; Wilson, D. A. Supramolecular Adaptive Nanomotors with Magnetotaxis Behavior. *Adv. Mater.* **2017**, *29* (6), 1604996.
(12) Joseph, A.; Contini, C.; Cecchin, D.; Nyberg, S.; Ruiz-Perez, L.; Gaitzsch, J.; Fullstone, G.; Tian, X.; Azizi, J.; Preston, J.; Volpe, G.; Battaglia, G. Chemotactic Synthetic Vesicles: Design and Applications in Blood-Brain Barrier Crossing. *Sci. Adv.* **2017**, *3* (8), e1700362.
(13) Li, J.; Thamphiwatana, S.; Liu, W.; Esteban-Fernández De Ávila, B.; Angsantikul, P.; Sandraz, E.; Wang, J.; Xu, T.; Soto, F.; Ramez, V.; Wang, X.; Gao, W.; Zhang, L.; Wang, J. Enteric Micromotor Can. Selectively Position and Spontaneously Propel in the Gastrointestinal Tract. *ACS Nano* **2016**, *10* (10), 9536−9542.
(14) Zhang, H.; Li, Z.; Wu, Z.; He, Q. Cancer Cell Membrane-Camouflaged Micromotor. *Adv. Ther (Weinh)* **2019**, *2* (12), 1900096.
(15) Gao, C.; Wang, Y.; Ye, Z.; Lin, Z.; Ma, X.; He, Q. Biomedical Micro- Nanomotors From Overcoming Biological Barriers to In Vivo Imaging. *Adv. Mater.* **2021**, *33*, 2000512.
(16) Chen, Y.; Pan, R.; Wang, Y.; Guo, P.; Liu, X.; Ji, F.; Hu, J.; Yan, X.; Wang, G. P.; Zhang, L.; Sun, Y.; Ma, X. Carbon Helical Nanorobots Capable of Cell Membrane Penetration for Single Cell Targeted SERS Bio-Sensing and Photothermal Cancer Therapy. *Adv. Funct Mater.* **2022**, *32* (30), 2200600.
(17) Li, J.; Angsantikul, P.; Liu, W.; Esteban-Fernández de Ávila, B.; Chang, X.; Sandraz, E.; Liang, Y.; Zhu, S.; Zhang, Y.; Chen, C.; Gao, W.; Zhang, L.; Wang, J. Biomimetic Platelet-Camouflaged Nanorobots for Binding and Isolation of Biological Threats. *Adv. Mater.* **2018**, *30* (2), 1704800.
(18) Wu, Z.; Troll, J.; Jeong, H. H.; Wei, Q.; Stang, M.; Ziemssen, F.; Wang, Z.; Dong, M.; Schnichels, S.; Qiu, T.; Fischer, P. A Swarm of Slippery Micropropellers Penetrates the Vitreous Body of the Eye. *Sci. Adv.* **2018**, *4* (11), 1−11.
(19) Walker, D.; Käsdorf, B. T.; Jeong, H.-H.; Lieleg, O.; Fischer, P. Enzymatically Active Biomimetic Micropropellers for the Penetration of Mucin Gels. *Sci. Adv.* **2015**, *1* (11), 33−35.
(20) Tang, S.; Zhang, F.; Gong, H.; Wei, F.; Zhuang, J.; Karshalev, E.; Esteban-Fernandez de Avila, B.; Huang, C.; Zhou, Z.; Li, Z.; Yin, L.; Dong, H.; Fang, R. H.; Zhang, X.; Zhang, L.; Wang, J. Enzyme-Powered Janus Platelet Cell Robots for Active and Targeted Drug Delivery. *Sci. Robot* **2020**, *5* (43), 6545−6557.
(21) Xuan, M.; Shao, J.; Gao, C.; Wang, W.; Dai, L.; He, Q. Self-Propelled Nanomotors for Thermomechanically Percolating Cell Membranes. *Angewandte Chemie - International Edition* **2018**, *57* (38), 12463−12467.
(22) Zhou, X.; Huang, X.; Wang, B.; Tan, L.; Zhang, Y.; Jiao, Y. Light/Gas Cascade-Propelled Janus Micromotors That Actively Overcome Sequential and Multi-Staged Biological Barriers for Precise Drug Delivery. *Chemical Engineering Journal* **2021**, *408*, 127897.
(23) Shao, J.; Cao, S.; Williams, D. S.; Abdelmohsen, L. K. E. A.; Hest, J. C. M. Photoactivated Polymersome Nanomotors: Traversing Biological Barriers. *Angew. Chem., Int. Ed.* **2020**, *59* (39), 16918−16925.
(24) Ramos-Docampo, M. A.; Fernández-Medina, M.; Taipaleenmäki, E.; Hovorka, O.; Salgueirinõ, V.; Städler, B. Microswimmers with Heat Delivery Capacity for 3D Cell Spheroid Penetration. *ACS Nano* **2019**, *13* (10), 12192−12205.
(25) Chen, W.; Jiang, R.; Sun, X.; Chen, S.; Liu, X.; Fu, M.; Yan, X.; Ma, X. Self-Fueled Janus Nanomotors as Active Drug Carriers for Propulsion Behavior-Reinforced Permeability and Accumulation at the Tumor Site. *Chem. Mater.* **2022**, *34*, 7543.
(26) Wan, M.; Wang, Q.; Wang, R.; Wu, R.; Li, T.; Fang, D.; Huang, Y.; Yu, Y.; Fang, L.; Wang, X.; Zhang, Y.; Miao, Z.; Zhao, B.; Wang, F.; Mao, C.; Jiang, Q.; Xu, X.; Shi, D. Platelet-Derived Porous Nanomotor for Thrombus Therapy. *Sci. Adv.* **2020**, *6* (22), eaaz9014.
(27) Shao, J.; Abdelghani, M.; Shen, G.; Cao, S.; Williams, D. S.; van Hest, J. C. M. Erythrocyte Membrane Modified Janus Polymeric Motors for Thrombus Therapy. *ACS Nano* **2018**, *12* (5), 4877−4885.
(28) Fang, D.; Li, T.; Wu, Z.; Wang, Q.; Wan, M.; Zhou, M.; Mao, C. Dual Drive Mode Polydopamine Nanomotors for Continuous Treatment of an Inferior Vena Cava Thrombus. *J. Mater. Chem. B* **2021**, *9* (41), 8659−8666.
(29) Teirlinck, E.; Xiong, R.; Brans, T.; Forier, K.; Fraire, J.; van Acker, H.; Matthijs, N.; de Rycke, R.; de Smedt, S. C.; Coenye, T.; Braeckmans, K. Laser-Induced Vapour Nanobubbles Improve Drug Diffusion and Efficiency in Bacterial Biofilms. *Nat. Commun.* **2018**, *9* (1), 4518.
(30) Teirlinck, E.; Barras, A.; Liu, J.; Fraire, J. C.; Lajunen, T.; Xiong, R.; Forier, K.; Li, C.; Urtti, A.; Boukherroub, R.; Szunerits, S.; De Smedt, S. C.; Coenye, T.; Braeckmans, K. Exploring Light-Sensitive Nanocarriers for Simultaneous Triggered Antibiotic Release and Disruption of Biofilms Upon Generation of Laser-Induced Vapor Nanobubbles. *Pharmaceutics* **2019**, *11*, 201.
(31) Sauvage, F.; Fraire, J. C.; Remaut, K.; Sebag, J.; Peynshaert, K.; Harrington, M.; van de Velde, F. J.; Xiong, R.; Tassignon, M.-J.; Brans, T.; Braeckmans, K.; de Smedt, S. C. Photoablation of Human Vitreous Opacities by Light-Induced Vapor Nanobubbles. *ACS Nano* **2019**, *13* (7), 8401−8416.
(32) Sauvage, F.; Nguyen, V. P.; Li, Y.; Harizaj, A.; Sebag, J.; Roels, D.; Van Havere, V.; Peynshaert, K.; Xiong, R.; Fraire, J. C.; Tassignon, M.-J.; Remaut, K.; Paulus, Y. M.; Braeckmans, K.; De Smedt, S. C. Laser-Induced Nanobubbles Safely Ablate Vitreous Opacities in Vivo. *Nat. Nanotechnol* **2022**, *17*, 552.
(33) Mathesh, M.; Sun, J.; Wilson, D. A. Enzyme Catalysis Powered Micro/Nanomotors for Biomedical Applications. *J. Mater. Chem. B* **2020**, *8* (33), 7319−7334.
(34) Arqué, X.; Romero-Rivera, A.; Feixas, F.; Patiño, T.; Osuna, S.; Sánchez, S. Intrinsic Enzymatic Properties Modulate the Self-Propulsion of Micromotors. *Nat. Commun.* **2019**, *10* (1), 1−12.
(35) Dey, K. K.; Zhao, X.; Tansi, B. M.; Méndez-Ortiz, W. J.; Córdova-Figueroa, U. M.; Golestanian, R.; Sen, A. Micromotors Powered by Enzyme Catalysis. *Nano Lett.* **2015**, *15* (12), 8311−8315.
(36) Choi, H.; Cho, S. H.; Hahn, S. K. Urease-Powered Polydopamine Nanomotors for Intravesical Therapy of Bladder Diseases. *ACS Nano* **2020**, *14* (6), 6683−6692.
(37) Hortelao, A. C.; Simó, C.; Guix, M.; Guallar-Garrido, S.; Julián, E.; Vilela, D.; Rejc, L.; Ramos-Cabrer, P.; Cossío, U.; Gómez-Vallejo, V.; Patiño, T.; Llop, J.; Sánchez, S. Swarming Behavior and in Vivo Monitoring of Enzymatic Nanomotors within the Bladder. *Sci. Robot* **2021**, *6* (52), No. eabd2823.
(38) Harizaj, A.; van Hauwermeiren, F.; Stremersch, S.; de Rycke, R.; de Keersmaecker, H.; Brans, T.; Fraire, J. C.; Grauwen, K.; de Smedt, S. C.; Lentacker, I.; Lamkanfi, M.; Braeckmans, K. Nanoparticle-Sensitized Photoporation Enables Inflammasome Activation Studies in Targeted Single Cells. *Nanoscale* **2021**, *13* (13), 6592−6604.
(39) Fraire, J. C.; Shaabani, E.; Sharifiaghdam, M.; Rombaut, M.; Hinnekens, C.; Hua, D.; Ramon, J.; Raes, L.; Bolea-Fernandez, E.; Brans, T.; Vanhaecke, F.; Borghgraef, P.; Huang, C.; Sauvage, F.; Vanhaecke, T.; de Kock, J.; Xiong, R.; de Smedt, S.; Braeckmans, K. Light Triggered Nanoscale Biolistics for Efficient Intracellular

https://doi.org/10.1021/acsnano.2c09380
ACS Nano 2023, 17, 7180−7193

Delivery of Functional Macromolecules in Mammalian Cells. *Nat. Commun.* **2022**, *13* (1), 1996.
(40) Patiño, T.; Feiner-Gracia, N.; Arqué, X.; Miguel-López, A.; Jannasch, A.; Stumpp, T.; Schäffer, E.; Albertazzi, L.; Sánchez, S. Influence of Enzyme Quantity and Distribution on the Self-Propulsion of Non-Janus Urease-Powered Micromotors. *J. Am. Chem. Soc.* **2018**, *140* (25), 7896−7903.
(41) de Corato, M.; Arqué, X.; Patinõ, T.; Arroyo, M.; Sánchez, S.; Pagonabarraga, I. Self-Propulsion of Active Colloids via Ion Release: Theory and Experiments. *Phys. Rev. Lett.* **2020**, *124* (10), 108001.
(42) Liu, L.; Mo, H.; Wei, S.; Raftery, D. Quantitative Analysis of Urea in Human Urine and Serum by 1H Nuclear Magnetic Resonance. *Analyst* **2012**, *137* (3), 595−600.
(43) Patino, T.; Arqué, X.; Mestre, R.; Palacios, L.; Sánchez, S. Fundamental Aspects of Enzyme-Powered Micro- and Nanoswimmers. *Acc. Chem. Res.* **2018**, *51* (11), 2662−2671.
(44) Hortelão, A. C.; García-Jimeno, S.; Cano-Sarabia, M.; Patiño, T.; Maspoch, D.; Sanchez, S. LipoBots: Using Liposomal Vesicles as Protective Shell of Urease-Based Nanomotors. *Adv. Funct Mater.* **2020**, *30* (42), 2002767.
(45) Raes, L.; Stremersch, S.; Fraire, J. C.; Brans, T.; Goetgeluk, G.; de Munter, S.; van Hoecke, L.; Verbeke, R. Intracellular Delivery of MRNA in Adherent and Suspension Cells by Vapor Nanobubble Photoporation. *Nanomicro Lett.* **2020**, *12* (1), 185.
(46) Fraire, J. C.; Houthaeve, G.; Liu, J.; Raes, L.; Vermeulen, L.; Stremersch, S.; Brans, T.; García-Díaz Barriga, G.; de Keulenaer, S.; van Nieuwerburgh, F.; de Rycke, R.; Vandesompele, J.; Mestdagh, P.; Raemdonck, K.; de Vos, W. H.; de Smedt, S.; Braeckmans, K. Vapor Nanobubble Is the More Reliable Photothermal Mechanism for Inducing Endosomal Escape of SiRNA without Disturbing Cell Homeostasis. *J. Controlled Release* **2020**, *319*, 262−275.
(47) Sun, B. The Mechanics of Fibrillar Collagen Extracellular Matrix. *Cell Rep. Phys. Sci.* **2021**, *2* (8), 100515.
(48) Barras, A.; Sauvage, F.; de Hoon, I.; Braeckmans, K.; Hua, D.; Buvat, G.; Fraire, J. C.; Lethien, C.; Sebag, J.; Harrington, M.; Abderrahmani, A.; Boukherroub, R.; de Smedt, S.; Szunerits, S. Carbon Quantum Dots as a Dual Platform for the Inhibition and Light-Based Destruction of Collagen Fibers: Implications for the Treatment of Eye Floaters. *Nanoscale Horiz* **2021**, *6* (6), 449−461.
(49) Gao, C.; Wang, Y.; Ye, Z.; Lin, Z.; Ma, X.; He, Q. Biomedical Micro-/Nanomotors: From Overcoming Biological Barriers to In Vivo Imaging. *Adv. Mater.* **2021**, *33* (6), 2000512.
(50) Xiong, R.; Xu, R. X.; Huang, C.; de Smedt, S.; Braeckmans, K. Stimuli-Responsive Nanobubbles for Biomedical Applications. *Chem. Soc. Rev.* **2021**, *50* (9), 5746−5776.
(51) Vermeulen, L. M. P.; Fraire, J. C.; Raes, L.; de Meester, E.; de Keulenaer, S.; van Nieuwerburgh, F.; de Smedt, S.; Remaut, K.; Braeckmans, K. Photothermally Triggered Endosomal Escape and Its Influence on Transfection Efficiency of Gold-Functionalized JetPEI/PDNA Nanoparticles. *Int. J. Mol. Sci.* **2018**, *19* (8), 2400.
(52) Das, A.; Mukhopadhyay, C. Urea-Mediated Protein Denaturation: A Consensus View. *J. Phys. Chem. B* **2009**, *113* (38), 12816−12824.
(53) Hortelão, A. C.; Patiño, T.; Perez-Jiménez, A.; Blanco, À.; Sánchez, S. Enzyme-Powered Nanobots Enhance Anticancer Drug Delivery. *Adv. Funct Mater.* **2018**, *28* (25), 1705086.
(54) Fraire, J. C.; Houthaeve, G.; Liu, J.; Raes, L.; Vermeulen, L.; Stremersch, S.; Brans, T.; García-Díaz Barriga, G.; de Keulenaer, S.; van Nieuwerburgh, F.; de Rycke, R.; Vandesompele, J.; Mestdagh, P.; Raemdonck, K.; de Vos, W. H.; de Smedt, S.; Braeckmans, K. Vapor Nanobubble Is the More Reliable Photothermal Mechanism for Inducing Endosomal Escape of SiRNA without Disturbing Cell Homeostasis. *J. Controlled Release* **2020**, *319*, 262−275.

https://doi.org/10.1021/acsnano.2c09380
ACS Nano 2023, 17, 7180−7193